A greener route to photoelectrochemically active PbS nanoparticles†

Javeed Akhtar,[a] M. Azad Malik,[a] Paul O'Brien,*[a] K. G. U. Wijayantha,[b] R. Dharmadasa,[b]
Samantha J. O. Hardman,[c] Darren M. Graham,[c] Ben F. Spencer,[cd] Stuart K. Stubbs,[c] Wendy R. Flavell,[c]
David J. Binks,[c] Fausto Sirotti,[e] Mario El Kazzi[e] and Mathieu Silly[e]

A cheap and more environmentally friendly method for the synthesis of high quality PbS nanoparticles in olive oil at 60 °C has been developed. Carefully controlling the conditions of reactions leads to PbS nanoparticles with well-defined sizes, and band gaps between 1.72 and 0.88 eV. The nanoparticles were characterized by XRD, HRTEM, NIR absorption spectroscopy, X-ray photoelectron spectroscopy (XPS) and a fluorescence lifetime experiment based on the time-correlated single photon counting (TCSPC) technique. Photoelectrochemical study carried out by steady-state current–voltage measurements of self-assembled PbS nanoparticles on ZnO–SnO$_2$ electrodes in 1 M Na$_2$SO$_3$ electrolyte solution showed that as-prepared PbS nanoparticles were photochemically active.

Introduction

Greener chemical methods are increasingly used for chemical synthesis[1–5] including those of inorganic nanomaterials.[6–10] A set of 12 principles for greener synthesis was defined by Anastas and Warner, these can be used as a guide by the synthetic chemist.[11–19] The driving force for such work in nanomaterials synthesis includes: minimizing chemical hazards to health, reducing eco-toxicity, a need for a competitive high quality products and using energy efficient chemical processes. In line with these ideas green nanochemistry attempts to develop methods to synthesize nanomaterials without using auxiliary solvents and/or surfactants thus leading to more environmentally benign nano-materials, potentially with reduced toxicity.[20,21]

PbS is an important direct band gap semiconductor material with a small band gap (0.41 eV)[22] and finds applications in near-IR communications.[23] It has a large Bohr radius (18 nm),[22] high dielectric constant (18)[22] and very high carrier mobility (0.44 Cm^2 V^{-1}·S^{-1}).[23] These properties lead to a third order nonlinear optical response some 30 times that of GaAs and 1000 times that of CdS nanoparticles for particles of similar size.[22] These features make PbS nanoparticles particularly suitable in optical and photonic device applications.[23,24] Near-infrared (NIR) emitting nanocrystals have also been used as biological labels, and as light harvesters.[25,26] Lead sulfide nanoparticles can also show multiple exciton generation (MEG), in which the impact of a single photon produces two or more excitons.[27–31] This phenomenon has raised the possibility of quantum dot based solar cells with photoconversion efficiency of as much as 66%.[32–37] It is also an attractive candidate for constructing such cells due to the fact that its band gap can be tuned across visible to NIR region (700–1600 nm).

Several synthetic methods have been used for the preparation of PbS nanoparticles.[38–45] However, the rapid injection of precursor(s) into hot coordinating solvents remains the most common method with quite good control of size and reproducibility being routinely attained. The injection methods often use trioctylphosphine (TOP) or tributylphosphine (TBP), trioctylphosphine oxide (TOPO) or oleylamine (OA) and other long chain amines as solvents and capping agents. The use of TOPO and other organic capping agents has been shown to enhance the toxicity of nanoparticles *in vivo* applications.[46–48] Poor surface passivation and photosensitivity with capping agents such as TOPO and thiol can accelerate the degradation of nanoparticles after their preparation.[49–52] Additionally, TOP and TBP are quite hazardous and unstable. One solution to this problem is to use ionic liquids as solvent for synthesis.[53–58] This approach also suffers from a number of drawbacks such as the requirement of capping agents, the high cost of ionic liquids and low solubility in these media of many precursors that are generally available.

Herein we report the synthesis of PbS nanoparticles in olive oil as an alternative to conventional organic capping agents and solvents. Olive oil is principally a triacylglyceride of long chain fatty acids including oleic, linoleic and linolenic acids; additional minor components are monoterpenes and long chain phenolic esters.[59–72] The use of olive oil as a capping agent and solvent eliminates the need for the use of air-sensitive, toxic and expensive chemicals such as TOP, TBP or amines. This method can easily be scaled for the gram scale synthesis of nanoparticles. To the best of our knowledge, there are no reports of the synthesis of PbS nanoparticles at such a low temperature (60 °C) in green solvent.

[a]School of Chemistry and Materials Science Centre, The University of Manchester, Oxford Road, Manchester, UK M13 9PL. E-mail: paul. obrien@manchester.ac.uk
[b]Department of Chemistry, Loughborough University, Loughborough, Leicestershire, UK LE11 3TU
[c]School of Physics and Astronomy and the Photon Science Institute, The University of Manchester, Oxford Road, Manchester, UK M13 9PL
[d]The Cockcroft Institute of Accelerator Science and Technology, STFC Daresbury laboratory, Daresbury, Warrington, Cheshire, WA4 4AD, UK
[e]TEMPO Beamline, Socité civile Synchrotron SOLEIL, L'Orme des Merisiers, Saint-Aubin - 48, 91192 Gif-sur-Yvette, France
† Electronic supplementary information (ESI) available: Composition of olive oil and IR-spectra of ligand exchange PbS nanoparticles. See DOI: 10.1039/b924436k

Experimental section

Materials

PbO (99.99%, Aldrich), olive oil (extra virgin, purchased from Tesco supermarket, see ESI† for composition of olive oil), TMS (bistrimethylsilyl sulfide), sulfur, potassium diethyl xanthate, lead acetate 99.9%, and mercaptopropionic acid (MPA, 99% purity) were obtained from Aldrich Chemicals. Acetone and toluene were distilled prior to use. Fluorine-doped tin oxide (FTO) coated glass substrates (TEC8, 8 Ω) were purchased from Pilkington.

General procedure for the synthesis of PbS nanoparticles

PbO (0.90 g, 3.75 mmol) was dissolved in 12.5 mL of olive oil, 1 mL of oleic acid and 1 mL of octadecene and heated to 150 °C under vacuum for 2 h. The flask was flushed with nitrogen and the injection temperature was adjusted to 60 °C. In another flask 100–600 μL (0.93–1.87 mmol) of TMS were dissolved in 2 mL of olive oil and 0.5 mL of octadecene kept under nitrogen for 30 min at room temperature. The rapid injection of TMS solution into the reaction flask changed the colour of the reaction mixture from colourless to brown-red and then to dark black depending on the growth time (10–180 s) as monitored by a stopwatch. The mixture was cooled to room temperature and 20 mL of anhydrous acetone were added to give a black precipitate of PbS nanoparticles which was separated by centrifugation for 10 min at 4000 rpm. The material obtained was then redispersed in dry toluene (5 mL) and re-precipitated by adding anhydrous acetone to wash off any excess olive oil. The purpose of the addition of oleic acid is to dissolve PbO completely while octadecene was added to decrease the viscosity of the mixture to induce uniform nucleation of nanoparticles. Elemental sulfur can be used instead of TMS as S^{2-} source.

Deposition of ZnO–SnO$_2$ composite films

The fluorine-doped tin oxide (FTO) coated glass substrates (Pilkington TEC8, 8 Ω) were washed in an ultrasonic bath with deionized water, propanol, acetone, and ethanol, and were then stored in ethanol until used. Nanocrystalline ZnO and ZnO–SnO$_2$ composite films were deposited by a combination of aerosol-assisted chemical vapour deposition (AACVD) and doctor-blade methods, followed by annealing of the films in air at 450 °C for 30 min. The average film thickness of nanocrystalline ZnO and ZnO–SnO$_2$ composite films was determined from cross-sectional SEM images, while the average particle radius was estimated (*ca.* 300 nm) by topographical SEM images.

Sensitization of PbS quantum dots to ZnO–SnO$_2$ composite films

ZnO–SnO$_2$ coated FTO substrates were placed in neat 3-mercaptopropanoic acid (10 mL) in 100 mL flask under N$_2$ atmosphere for 14 h. Due to high affinity of the –COOH group towards Lewis acid sites on oxide surface, –COOH groups adsorbed on the surface leaving –SH ends away from the surface. In another 100 mL flask 85 mg of PbS nanoparticles prepared in olive oil were dissolved under nitrogen in 10 mL of anhydrous toluene. After

14 h substrates were removed one by one and washed with dry toluene to remove excess of 3-mercaptopropanoic acid from the electrode surfaces. They were immediately placed in a dry toluene solution of PbS nanoparticles prepared in olive oil overnight. Within the first hour ZnO–SnO$_2$ surface turned brown in colour indicating the start of the sensitization process. The free –SH group has a high affinity towards PbS dots which will gradually replace triglycerides of olive oil from the surface of PbS dots, thus attaching the dots directly to the oxide surface *via* the –SH group of mercaptopropanoic acid as the linker.[73] On the completion of the sensitization process, the substrates were removed and washed with toluene to remove loosely attached PbS nanoparticles from the electrode surface. The sensitization process was carried out under N$_2$ and in the dark.

Photoelectrochemical (PEC) measurements

Photoelectrochemical measurements were conducted using a three-electrode configuration in 1 M Na$_2$SO$_3$ electrolyte, Ag/AgCl/KCl as reference electrode, and a platinum wire as the counter electrode. The potential of the photoelectrode was controlled by a potentiostat (microAutoLab, type III). In the electrochemical cell, light enters through a quartz window and travels about a 5 mm path length in the electrolyte before illuminating the photoelectrode. The PbS sensitized metal oxide electrodes were illuminated on the electrolyte side, and the illumination area was 0.8 cm^2. The illumination source was an AM1.5 class A solar simulator (Solar Light 16S—300 solar simulator) equipped with a 300 W xenon lamp. The intensity of the light was calibrated at 1000 W m^{-2} using a class II pyranometer (PMA2144, Solar Light Co., Inc.) equipped with a digital photometer (PMA2100, Solar Light Co., Inc.).

Characterization

X-Ray powder diffraction patterns were obtained using a Bruker D8 AXE diffractometer (Cu-Kα). TEM samples were prepared by evaporating a dilute toluene solution of the nanoparticles on carbon coated copper grids (S166-3, Agar Scientific) and a Philips Technai Transmission Electron microscope was used to obtain TEM images of the nanoparticles. X-Ray photoemission spectroscopy was performed on the PbS nanocrystals on the TEMPO beamline at SOLEIL, France. Photoluminescence (PL) lifetime measurements were performed using a commercial instrument (MiniTau, Edinburgh Instruments) which utilizes the time-correlated single photon counting technique and bandpass filters to spectrally isolate the PL. Due to the spectral sensitivity of the photomultiplier tube used (Hamamatsu R3809U-50) only the PL at wavelengths shorter than about 850 nm could be detected, therefore two samples with exciton peaks less than 850 nm were used. Samples were excited by a pulsed diode laser (EPL-405) which emitted a wavelength of 405 nm with pulse duration of 90 ps. The steady-state current–voltage characteristics of PbS self-assembled ZnO–SnO$_2$ electrodes were studied in 1 M Na$_2$SO$_3$ electrolyte solution.

Results and discussion

Experiments were performed under different conditions of [Pb] : [S] mole ratio and growth time, in order to determine the
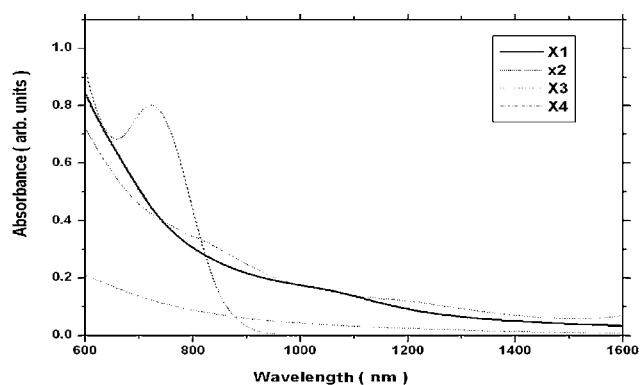
This journal is © The Royal Society of Chemistry 2010

J. Mater. Chem., 2010, **20**, 2336–2344 | 2337

Fig. 1 Room temperature absorption spectra of PbS nanoparticles prepared at 60 °C for X1–X4 with growth time of 30 s.

Table 1 Band gap and average size distribution with standard deviation of PbS nanoparticles prepared at 60 °C of all four samples X4–X7 (calculations based on 100 nanoparticles in TEM images)

Experiments	Growth time/s	Mean diameter^a/nm	Transition energy $1S_e$–$1S_h$/eV	PL peak position/eV
X4	30	2.79 ± 0.2	1.71	1.34
X5	60	3.80 ± 0.2	1.35	1.21
X6	120	4.44 ± 0.3	1.15	1.06
X7	180	5.22 ± 0.6	0.88	0.85

^{a} Mean diameter calculated from TEM.

optimum conditions for PbS nanoparticles synthesis. The first set of experiments (X1–X4) was carried out to determine the effect of the [Pb] : [S] mole ratio on the size or the quality of the nanoparticles. The ratio of [Pb] : [S] was varied in the reaction mixture (PbO : TMS) from 1 : 2 to 1 : 0.25 at 60 °C for 30 s growth time. The highest molar ratio [Pb] : [S] (1 : 2) in the reaction mixture (X1) produced a product with negligible absorption with a flat line in the absorption spectrum (Fig. 1 (X1)). In the second experiment (X2) the [Pb] : [S] ratio was reduced to 1 : 1. The nanoparticles produced from this reaction showed a broad absorption spectrum with a long tail without any excitonic feature indicative of a broad size distribution (Fig. 1 (X3)). In the third experiment (X3) the ratio of [Pb] : [S] was 1 : 0.5. The absorption spectrum showed a broad hump around 860 nm but with as much long tail as for the sample with a 1 : 1 ratio (Fig. 1 (X2)). In the fourth experiment (X4) the [Pb] : [S] ratio
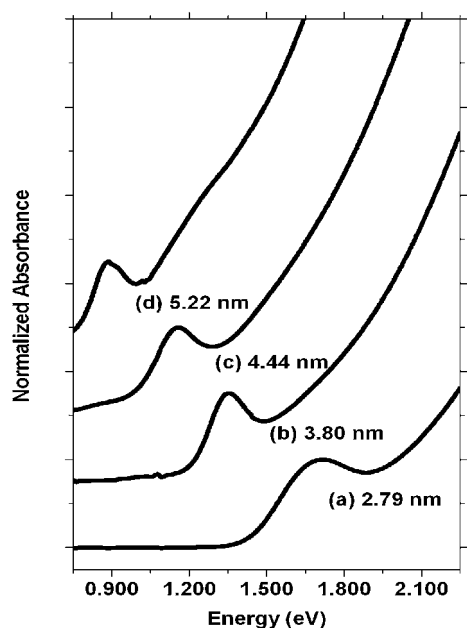
was 1 : 0.25. The resultant nanoparticles gave an absorption spectrum with a prominent shoulder for first exciton around 720 nm and a sharp peak (Fig. 1 (X4)).

The other important factor in controlling the size of the nanoparticles was the growth time. A separate set of experiments (X4–X7) was carried out with a precursor mixture containing a [Pb] : [S] molar ratio of 1 : 0.25 at 60 °C for 30, 60, 120 and 180 s of growth time (Fig. 2a–d). The nanoparticles produced at 30 s (X4) showed a clean and narrow absorption spectrum with a peak corresponding to the first exciton around 720 nm (1.719 eV) (Fig. 2a). By increasing the growth time to 60 s (X5) the excitonic peak shifted to 920 nm (1.35 eV) (Fig. 2b). The absorption spectrum of PbS nanoparticles grown for 120 s (X6) further shifted the peak to 1180 nm (1.15 eV) (Fig. 2c). Similarly, the PbS nanoparticles prepared with a growth time of 180 s (X7) showed some additional features due to higher energy transitions within the nanoparticles in addition to the excitonic peak at
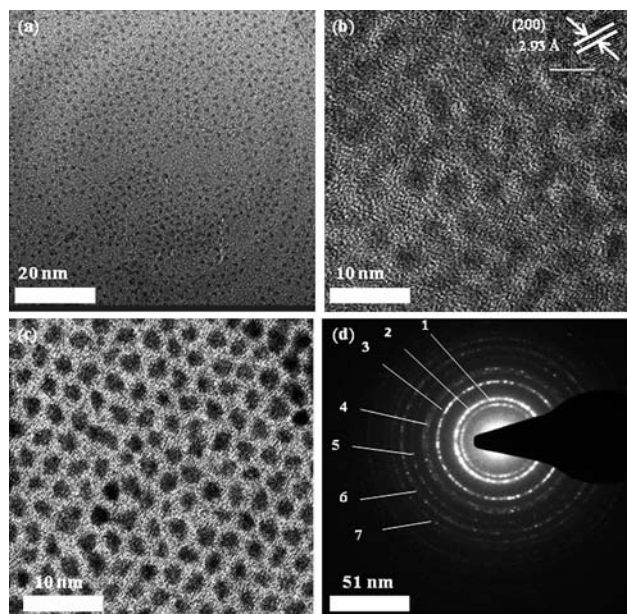

Fig. 2 Room temperature absorption spectra of PbS nanoparticles prepared at 60 °C using Pb : S mole ratio, 1 : 0.25 (a) X4, growth time 30 s, (b) X5, growth time 60 s, (c) X6, growth time 120 s and (d) X7, growth time 180 s.

Fig. 3 TEM of PbS nanoparticles of (a) sample X4, growth time 30 s, (b) HRTEM of PbS nanoparticles sample X6, growth time 120 s, insert showing lattice fringes of cubic PbS nanoparticle, $d = 2.93$ Å and calculated corresponding plan (200), (ICCD-5-592), (c) TEM of PbS nanoparticles of sample X7, growth time 180 s and (d) SAED pattern of PbS nanoparticle, the diffraction rings match the PbS cubic phase and labelled rings have been identified as 1. (111), 2. (200), 3. (220), 4. (311), 5. (222), 6. (400), 7. (420).
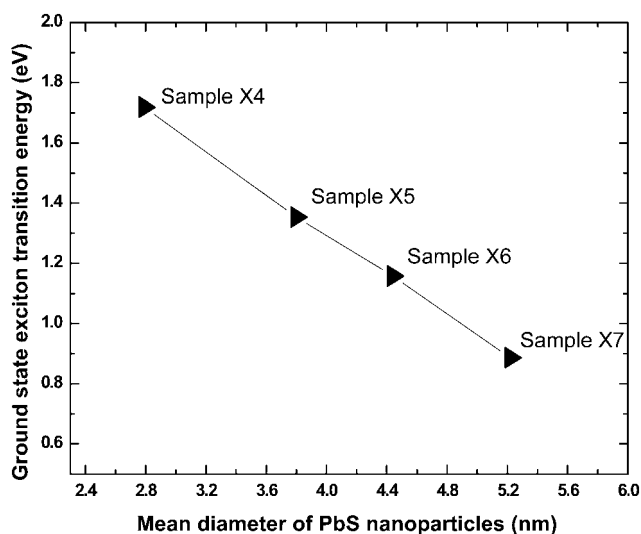
Fig. 4 Variation of the ground state exciton transition energy with the mean particle diameter determined from TEM (line is drawn for clarity). This graph shows dependence of the exciton transition energy on the size of nanoparticles (calculations based on 100 nanoparticles in TEM images).

1410 nm (0.88 eV) (Fig. 2d). It is clear from Fig. 2 that a large quantum confinement induced blue shift of the absorption edge of the PbS nanoparticles to occur with decreasing reaction time.

The ground state excitonic transition energies, determined from the positions of the first excitonic absorption peak in Fig. 2, are 1.71 eV, 1.35 eV, 1.15 eV and 0.88 eV for samples (X4–X7) respectively (Table 1) showing that the band gap can be tuned across the whole of the near-infrared spectral region from 720 nm to 1410 nm which is consistent with the data reported by Cademartiri and co-workers.[74]

Transmission electron microscopy (TEM) analysis of all four samples (X4–X7) of PbS nanoparticles was carried out to observe the shape and calculate the diameter of the as-prepared nanoparticles. The shape of the PbS nanoparticles was close to spherical in all cases as shown in Fig. 3a–c. This figure also
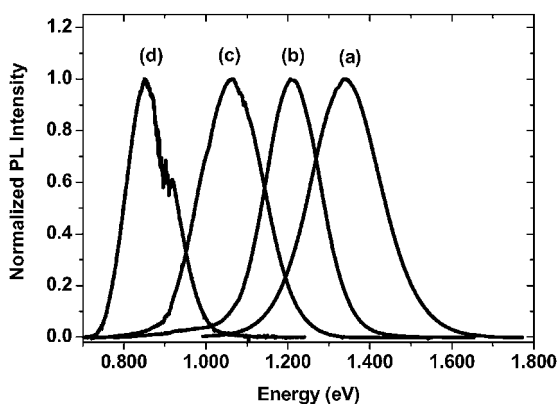
provides insights into the crystal structures of these nanoparticles. HRTEM lattice fringe images (Fig. 3b and corresponding insert) showed single crystals with few defects. The lattice spacing was calculated as 2.93 Å, which corresponds to the interlayer separation along the (200) lattice plane for bulk PbS (ICCD-5-592). Furthermore, the selected area electron diffraction (SAED) patterns index well to the cubic rock salt PbS crystal structure (Fig. 3d) and diffraction rings matched well with corresponding XRD patterns of the PbS nanoparticles.

Fig. 4 shows the relationship between the ground state exciton transition energy and the mean particle diameter of the PbS nanoparticles determined from HRTEM images. Sharp absorption peaks in Fig. 2 also indicate the little polydispersity in the nanoparticle samples. This good size distribution is obtained without any post-synthesis size selective precipitation. Compared to other methods[38–45] where post-reaction size selective

Fig. 5 Normalized room temperature photoluminescence spectra of PbS nanoparticles prepared at 60 °C, using Pb : S mole ratio, 1 : 0.25 (a) X4, growth time 30 s, (b) X5, growth time 60 s, (c) X6, growth time 120 s and (d) X7, growth time 180 s. The sharp features observed between 0.86 and 0.92 eV are due to absorption by atmospheric water vapour.
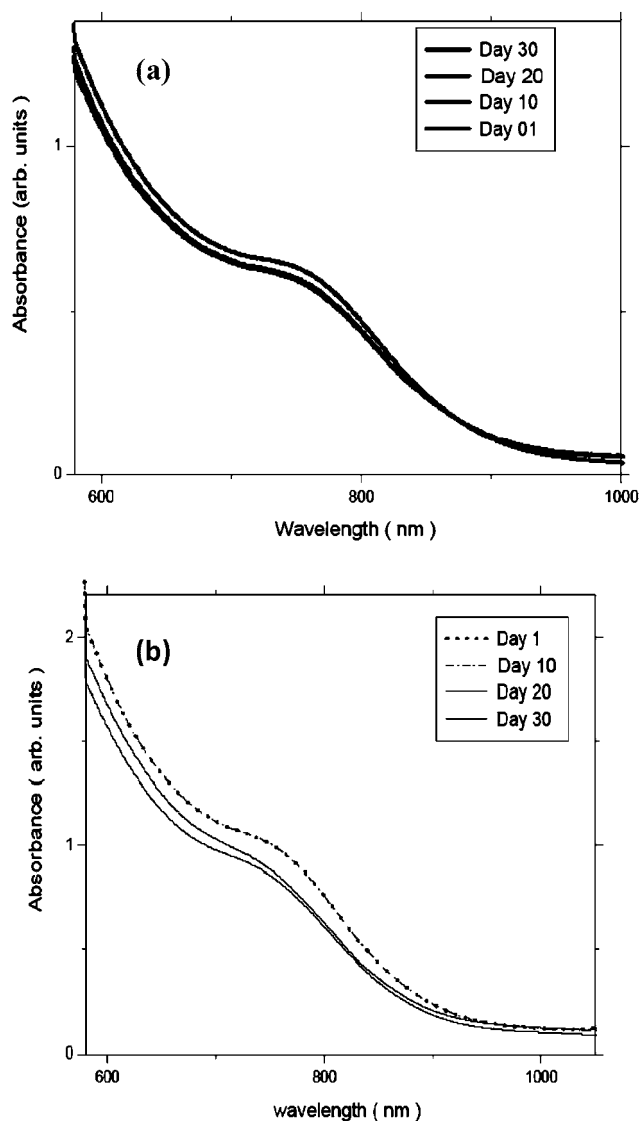

Fig. 6 Room temperature absorption spectra of PbS nanoparticles prepared at 60 °C, sample X3 (a) PbS nanoparticle in toluene kept under dark and (b) PbS nanoparticle toluene solution in light. PbS nanoparticles *N.B.* All spectra are normalized to the intensity of the ground state excitonic absorption peak and are vertically offset for clarity.

This journal is © The Royal Society of Chemistry 2010

J. Mater. Chem., 2010, **20**, 2336–2344 | 2339

precipitation is essential to obtain monodispersed nanoparticles, this method is simple. The room temperature photoluminescence spectra of PbS nanoparticles prepared at a [Pb] : [S] molar ratio of 1 : 0.25 at 60 °C for 30 s to 180 s of growth times (interval) are shown in Fig. 5. The PbS nanoparticles (X4) with an excitonic peak at 720 nm showed luminescence in NIR region at 925 nm (Fig. 5a). The full width at half-maximum (FWHM) height of the photoluminescence spectra is 197 meV (Fig. 5a). The PL spectrum of PbS nanoparticles grown for 60 s (X5) showed emission at 1025 nm (Fig. 5a) with an FWHM in the PL spectrum of 156 meV (Fig. 5b). The emission peaks for PbS nanoparticles prepared over 120 and 180 s occurred at 1170 nm (Fig. 5c) and 1460 nm (Fig. 5d) with corresponding FWHM of 180 meV (Fig. 5c) and 133 meV (Fig. 5d) respectively. These FWHM values are comparable with the values recently reported by Turyanska[75] and confirm the relatively small degree of polydispersity in the nanoparticles.

In order to study the stability of the PbS nanoparticles in toluene we monitored changes over time in the first excitonic peak. Two solutions of similar concentration (0.50 mg PbS nanoparticles (X3) in 20 ml of anhydrous toluene) were prepared. One solution was wrapped in black paper and kept under dark, whilst the other was kept in light under the ambient laboratory conditions. The absorption spectra of the two solutions were measured intermittently over a period of one month and are shown in Fig. 6. The presence of the first excitonic peak in the absorption spectrum without a significant change after 30 days, under both dark and light conditions clearly demonstrates that the PbS nanoparticles prepared by this method are relatively stable in toluene.

The XRD pattern of the as-prepared PbS nanoparticles (X1–X4) (Fig. 7) shows cubic PbS nanoparticles with a lattice parameter $a = 0.5918$ nm (ICCD-5-592). The characteristic peaks for (111), (200), (220), (331), (400) and (420) reflections can be clearly identified. The appearance of broad peaks is as expected for small size nanoparticles of PbS. The sizes of the PbS nanoparticles were estimated using the Scherrer equation as: 3.5 nm (X4), 4.3 nm (X5), 4.9 nm (X6) and 5.8 nm (X7). The estimated size from XRD is fairly close to the size as determined from transmission electron microscopy (TEM) analysis.

In order to study the chemical environment of PbS nanoparticles prepared in olive oil X-ray photoelectron spectroscopy (XPS) was carried out on the PbS nanoparticles prepared in experiment X4. The first study was attempted on olive oil capped PbS nanoparticles by casting a film on FTO coated glass substrate in toluene. However, due to the presence of the long insulating oleic acid alkyl chain, samples were subjected to charging in the XPS experiment. Therefore, ligand exchange with butyl amine was carried out (see ESI†) and butyl amine capped nanoparticles were then analyzed by XPS.

The XPS spectra showed the presence of Pb and S, as expected, and also C and N which are attributed to the capping ligands. Exposure to the air after synthesis had a significant effect on the spectra; adsorbed molecules from the atmosphere such as water and carbon dioxide contributed to the C and O peak intensities. Fig. 8 and 9 show high-resolution spectra of the Pb 4f and S 2p core levels. A Shirley type background was subtracted and Voigt functions used to fit the line shapes. The spin-orbit splitting of the doublets was set as 4.8 eV for the Pb 4f peaks and 1.2 eV for the S 2p peaks. The intensity ratio was set as 4 : 3 for the Pb 4f doublets
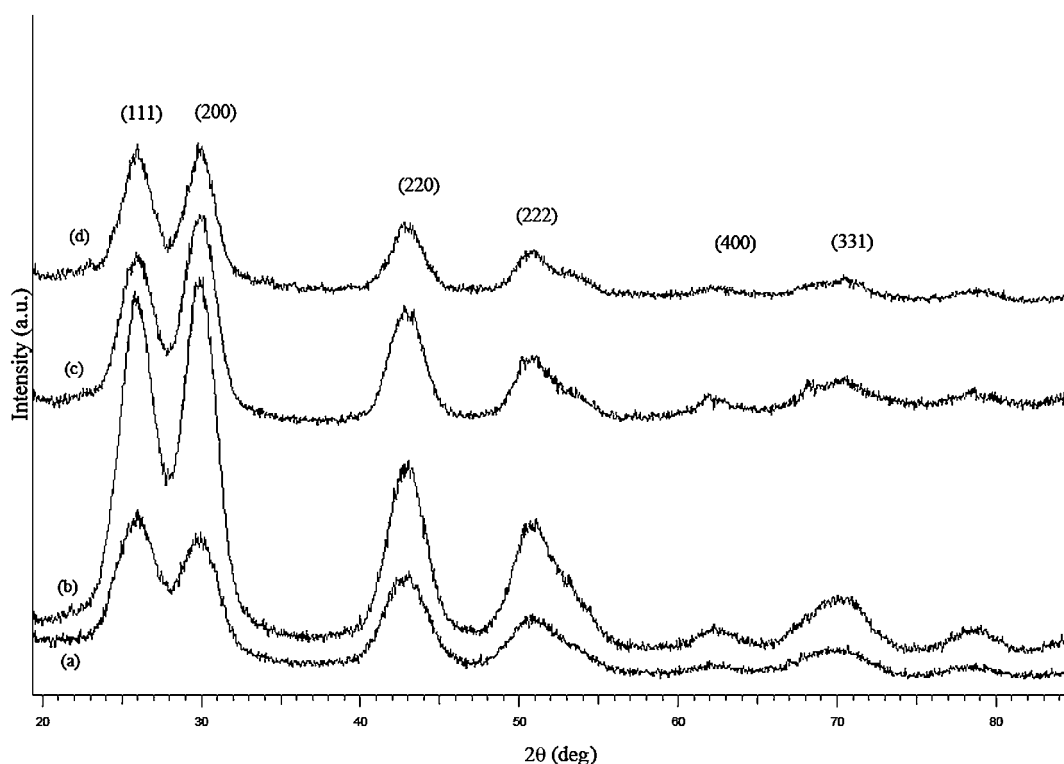

Fig. 7 XRD patterns of PbS nanoparticles prepared in olive oil at 60 °C using Pb : S mole ratio, 1 : 0.25 (a) X4, growth time 30 s (b) X5, growth time 60 s (c) X6, growth time 120 s and (d) X7, growth time 180 s for all four samples.
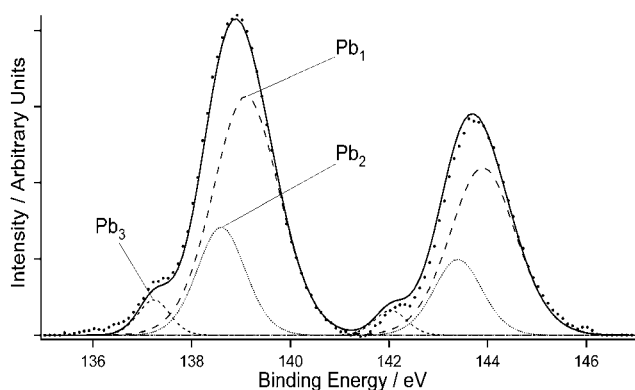
Fig. 8 X-Ray photoemission spectrum of lead 4f core levels. Doublet Pb$_1$ (long dashes) occurs at 139.1 and 143.9 eV, doublet Pb$_2$ (dots) occurs at 138.6 and 143.4 eV, doublet Pb$_3$ (short dashes) occurs at 137.2 and 142.0 eV (sample X4).
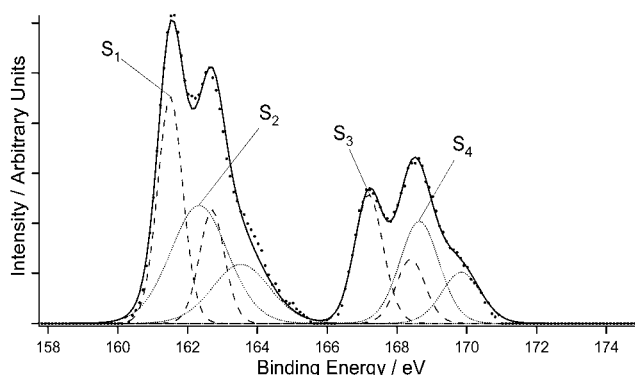

Fig. 9 X-Ray photoemission spectrum of sulfur 2p core levels. Doublet S$_1$ (long dashes) occurs at 161.5 and 162.7 eV, doublet S$_2$ (dots) occurs at 162.3 and 163.5 eV, doublet S$_3$ (long dashes) occurs at 167.2 and 168.4 eV, doublet S$_4$ (dots) occurs at 168.6 and 169.8 eV (sample X4).

and 2 : 1 for the S 2p doublets. The Pb 4f spectra show at least 3 components present in the sample, Pb1, Pb2 and Pb3, which are attributed to PbSO$_4$, PbS, and Pb respectively. The S 2p core level spectra show at least 4 components, S1, S2, S3 and S4, which are attributed to PbS, S, and highly oxidized states such as PbSO$_3$ and PbSO$_4$ respectively. The oxidized species present in the sample are due to exposure of the surfaces of the PbS nanocrystals to the air after synthesis. The reaction of surface molecules with the atmosphere is an effect which has been previously observed in PbS nanocrystals.[76] Using the areas of the Pb 4f and S 2p core level spectra and the photoionization cross-sections[77] the ratio of Pb to S was found to be 1.7 : 1 in the PbS nanocrystals. Similarly, high-resolution spectra of the valence band and Pb 5d core levels for both bulk PbS and the PbS nanocrystals are shown in Fig. 10. The apparent shift in the Pb 5d doublet from 18.9 and 21.5 eV in the bulk to 20.3 and 22.9 eV in the PbS nanocrystals is again due to the surface oxidation of the nanocrystals. The series of broad peaks in the PbS nanocrystal spectrum, which are most intense around 5–10 eV binding energy, are attributed to the nanocrystal capping groups. The binding energy of the edge of the valence band is equivalent to the gap between the Fermi level and the valence band of a substance. This value was measured as 0.35 eV for bulk PbS
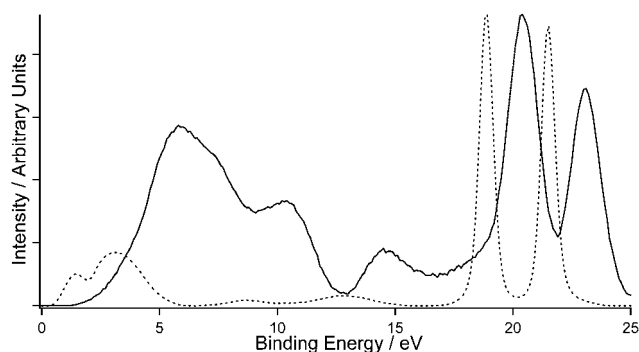

Fig. 10 X-Ray photoemission spectra of valence band and lead 5d core levels for bulk PbS (dashed line) and PbS nanocrystals (solid line, sample X4).

and 1.32 eV for the PbS nanocrystals. The band gap of bulk PbS has been measured to be 0.41 eV[22] whilst the band gap of the PbS nanocrystal samples was ~1.6 eV. This means that both the bulk sample and the PbS nanocrystals were n-type semiconductors.

A fluorescence lifetime experiment based on the time-correlated single photon counting (TCSPC) technique was carried out on as-prepared PbS nanoparticles. Samples X3 and X4 of PbS nanoparticles were analyzed by time-correlated single photon counting (TCSPC) and PL decay curves were monitored as shown in Fig. 11. In both cases, after the first microsecond the decay is largely mono-exponential with an associated time constant of ~1.2 μs, which is similar to previously reported PL lifetimes for PbS and can be attributed to band edge recombination. However, at times shorter than 1 μs the PL decay is multi-exponential, indicating that processes other than band edge recombination contribute significantly to the decay on this time-scale.[78] The long radiative lifetimes in the PbS nanocrystals are attributed to the dielectric screening. The screening of the radiating field inside the nanocrystal has the effect of weakening the internal field and consequently increasing the radiative lifetime. The long lifetimes associated with the effect of dielectric screening are predicted for all the IV–VI semiconductor nanocrystals with high dielectric constants recorded for long lifetimes.[79]

To investigate the photoelectrochemical behaviour of as-prepared PbS nanoparticles, they were assembled on the surface
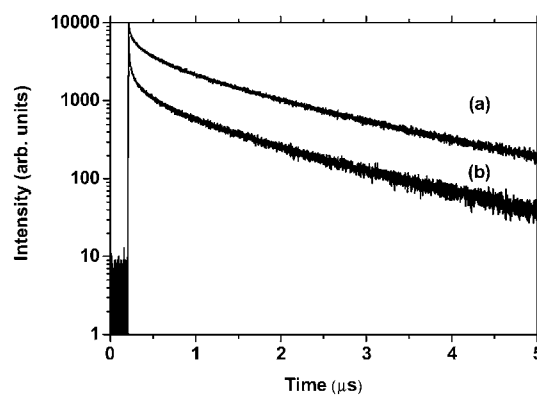

Fig. 11 Fluorescence lifetime decay curves of PbS nanoparticles prepared in olive oil at 60 °C (a) sample X3 and (b) X4.
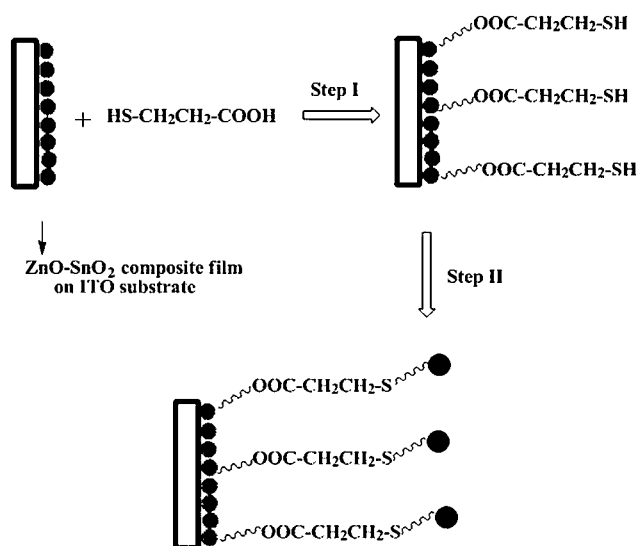
Fig. 12 Schematic representation of PbS nanoparticles sensitization process with 3-mercaptopropanoic acid with ZnO–SnO$_2$ composite film deposited on ITO, wavy lines indicate the chemical bonding. Step I—electrode is dipped in 3-mercaptopropanoic acid solution for 14 h. Step II—these electrodes were removed and washed with toluene to remove excess of acid and then dipped in PbS nanoparticles solution (sample X4).

of nanocrystalline ZnO–SnO$_2$ electrodes. The attachment of PbS nanoparticles on ZnO–SnO$_2$ surface was carried out by the adsorption process as depicted in Fig. 12. The steady-state current–voltage characteristics of PbS self-assembled ZnO–SnO$_2$ electrodes were studied in 1 M Na$_2$SO$_3$ electrolyte solution. Since the band gap of PbS is quite low (~0.41 eV for bulk PbS at 298 K),[22] it is essential to study photoelectrochemical properties of PbS by coupling to a wide band gap semiconductor material
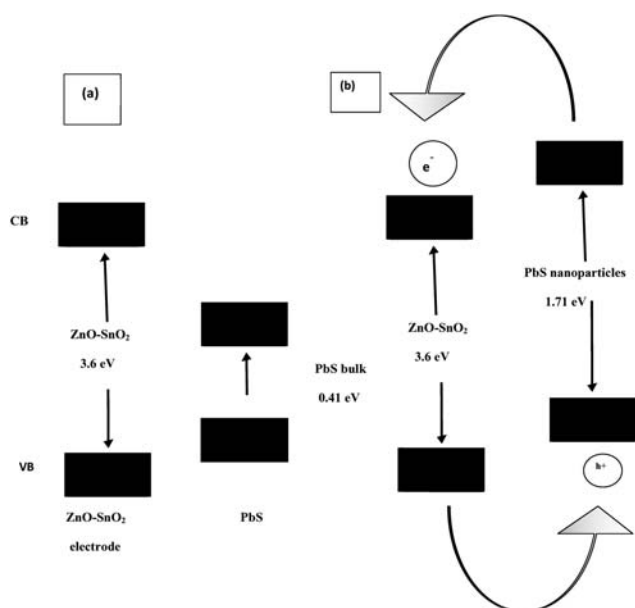
(*i.e.* ZnO, TiO$_2$) or suitable metal (*i.e.* Au) as a photosensitizer.[80–82] Both ZnO and SnO$_2$ are wide band gap semiconductor materials and absorb only a very small fraction of the visible light. Therefore, the electrodes made from either of those materials or the composite ZnO–SnO$_2$ electrodes show a negligible photocurrent under visible light. Nanocrystalline ZnO–SnO$_2$ composite electrodes used in this study have been already been employed to construct dye-sensitized solar cells successfully.[83–86]

The ZnO–SnO$_2$ electrode consisted of nanosized crystallites which provided a high surface area to facilitate attachment of PbS nanoparticles and absorb visible light. The band gap of PbS nanoparticles increases due to size quantization effect. The repositioning of the conduction band of PbS negative to that of ZnO–SnO$_2$ is a direct result of quantum confinement in PbS nanoparticles. Under these conditions the charge injection takes place from the conduction band of PbS into that of ZnO–SnO$_2$ as shown by schematics in Fig. 13. Once the photogenerated charges are injected, they transport through the metal oxide composite electrode and are subsequently collected at the FTO substrate. High-resolution SEM and AFM in Fig. 14 show the surface morphology of ZnO–SnO$_2$ composite electrode. Small needle-like structures grow up from the surface of the substrate at different angles, due to the uneven morphology of the FTO substrate. The photocurrent of the bare composite ZnO–SnO$_2$
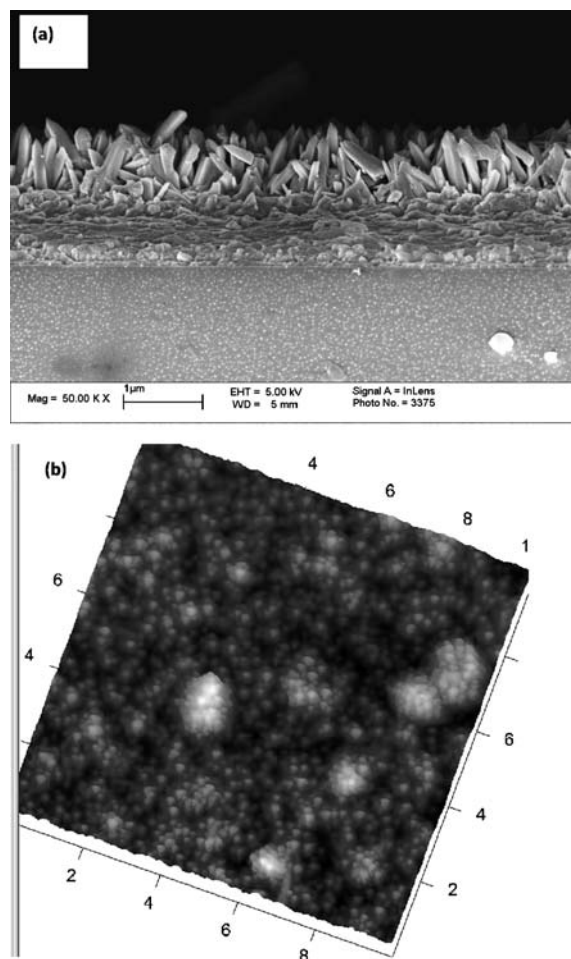

Fig. 13 Schematic band diagram of the quantum size PbS/ZnO–SnO$_2$ interface, also shown is the corresponding diagram for bulk PbS[22]. Based on ref. 86, the electron affinity and band gap of ZnO–SnO$_2$ are estimated to be 5.1 eV and 3.6 respectively. VB stands for valence band and CB stands for conduction band.

Fig. 14 High-resolution image of (a) SEM and (b) AFM image of composite ZnO–SnO$_2$ thin films.
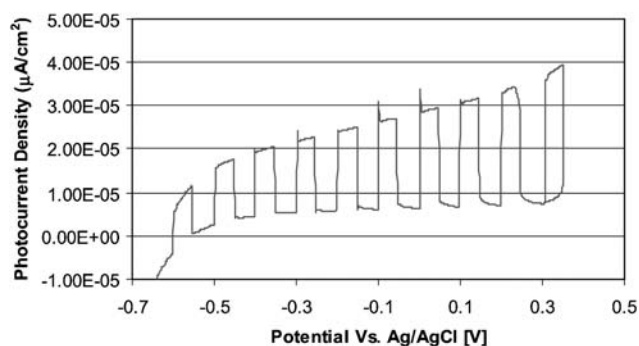
Fig. 15 Cyclic voltammogram of the PbS assembled nanoparticles on composite film of ZnO–SnO$_2$.

electrode as measured under AM1.5 simulated light is negligible (∼0.02 μA cm^{-2}) which indicates that charge generation in the high band gap metal oxide phase under visible light is very low. However, the PbS nanoparticles composite ZnO–SnO$_2$ electrode shows a significantly higher photocurrent density under the same illumination, suggesting the enhanced light absorption and charge injection after surface attachment of PbS quantum dots on metal oxide surface. The photocurrent onset is at about −0.6 V *vs.* the Ag/AgCl/KCl reference electrode potential in 1 M Na$_2$SO$_3$ aqueous electrolyte. The steady-state photocurrent density under AM1.5 illumination is 50 μA cm^{-2} as shown in Fig. 15.

Conclusion

We have described a simple and cheap synthetic route to high quality PbS nanoparticles in olive oil. The as-prepared nanoparticles are of fairly good homogeneity. They are stable and do not show any sign of decomposition over a period of many months. They have shown active photoelectrochemical behaviour. Further work is under way to study the detailed photoelectrochemical properties of such PbS nanoparticles.

Acknowledgements

References

1 J. F. Ang, Y. D. Wang, Z. W. Cui, F. Wang, Z. W. Miao and R. Y. Chen, *Heteroat. Chem.*, 2008, **19**, 596.
2 Q. Y. Zhang, B. K. Liu, W. Q. Chen, Q. Wu and X. F. Lin, *Green Chem.*, 2008, **10**, 972.
3 J. Xie, X. S. Zheng, A. Q. Dong, Z. D. Xiao and J. H. Zhang, *Green Chem.*, 2009, **11**, 355.
4 T. Ueda and H. Kotsuki, *Heterocycles*, 2008, **76**, 73.
5 M. Adib, M. Mahdavi, M. A. Noghani and P. Mirzaei, *Tetrahedron Lett.*, 2007, **48**, 7263.
6 P. Raveendran, J. Fu and S. L. Wallen, *J. Am. Chem. Soc.*, 2003, **125**, 13940.
7 K. Roy and S. Lahiri, *Green Chem.*, 2006, **8**, 1063.
8 S. Sapra, A. L. Rogach and J. Feldmann, *J. Mater. Chem.*, 2006, **16**, 3391.
9 W. Yang, Y. Ma, J. Tang and X. R. Yang, *Colloids Surf., A*, 2007, **302**, 33.
10 S. Y. Gao, Y. G. Shi, S. X. Zhang, K. Jiang, S. X. Yang, Z. D. Li and E. Takayama-Muromachi, *J. Phys. Chem. C*, 2008, **112**, 10398.
11 P. T. Anastas and J. C. Warner, *Green Chemistry: Theory and Practice*, Oxford University Press, New York, 1998, p. 30.
12 P. T. Anastas and M. A. Kirchhoff, *Acc. Chem. Res.*, 2002, **35**, 686.
13 P. T. Anastas and T. C. Williamson, *Green Chemistry: Frontiers in Benign Chemical Syntheses and Processes*, Oxford University Press, New York, 1998, p. 11.
14 W. Leitner, *Appl. Organomet. Chem.*, 2000, **14**, 809.
15 M. G. Hitzler and M. Poliakoff, *Chem. Commun.*, 1997, 1667.
16 G. W. Breton and C. A. Hughey, *J. Chem. Educ.*, 1998, **75**, 85.
17 S. Borman, *Chem. Eng. News*, 2001, **79**, 5.
18 Z. Y. J. Zou, K. Sayama and H. Arakawa, *Nature*, 2001, **414**, 625.
19 G. Kumar, J. F. Bristow, P. J. Smith and G. F. Payne, *Polymer*, 2000, **41**, 2157.
20 A. D. Jennifer, L. S. Bettye and E. H. James, *Chem. Rev.*, 2007, **107**, 2228.
21 L. C. McKenzie and J. E. Hutchison, *Chim. Oggi*, 2004, **22**, 30.
22 K. Inuk and W. W. Frank, *J. Opt. Soc. Am.*, 1997, **14**, 1639.
23 W. W. Scanlon, *Phys. Rev.*, 1958, **109**, 47.
24 W. W. Scanlon, *J. Phys. Chem. Solids*, 1959, **8**, 423.
25 G. I. Koleilat, L. Levina, H. Shukla, S. H. Myrskog, S. Hinds, A. G. Pattantyus and E. H. Sargent, *ACS Nano*, 2008, **2**, 833.
26 B. R. Saunders and M. L. Turner, *Adv. Colloid Interface Sci.*, 2008, **138**, 1.
27 R. J. Ellingson, M. C. Beard, J. C. Johnson, P. R. Yu, O. I. Micic, A. J. Nozik, A. Shabaev and A. L. Efros, *Nano Lett.*, 2005, **5**, 865.
28 I. K. Victor, *Annu. Rev. Phys. Chem.*, 2007, **58**, 635.
29 K. Sabine, H. W. Jugen, W. Thomas and J. Q. Hans, *Appl. Phys. Lett.*, 1993, **63**, 17.
30 D. S. Gregory and R. Garry, *Nat. Mater.*, 2006, **5**, 683.
31 G. Allan and C. Delerue, *Phys. Rev. B: Condens. Matter*, 2008, **77**, 125340.
32 K. Anusorn, T. Kevin, T. Kensuke, K. Masaru and V. K. Prashant, *J. Am. Chem. Soc.*, 2008, **130**, 4007.
33 G. Hodes, *Isr. J. Chem.*, 1993, **33**, 95.
34 G. Sasha and H. Gary, *J. Phys. Chem.*, 1994, **98**, 5338.
35 A. J. Nozik, *Physica E (Amsterdam)*, 2002, **14**, 115.
36 Z. L. Wang, *J. Phys. Chem.*, 2000, **104**, 1153.
37 K. Sandeep and D. S. Gregory, *Microchim. Acta*, 2008, **160**, 315.
38 L. Jincheng, Y. Huangzhong, W. Zhonglian, W. Wenli, P. Junbiao and C. Yong, *Nanotechnology*, 2008, **19**, 345602.
39 T. Trindade, P. O'Brien, Z. Xiao-mei and M. Majid, *J. Mater. Chem.*, 1997, **7**, 1011.
40 G. J. Zhou, M. K. Lu, Z. L. Xiu, S. F. Wang, H. P. Zhang, Y. Y. Zhou and S. M. Wang, *J. Phys. Chem. B*, 2006, **110**, 6543.
41 B. Deborah, G. Kuveshni, S. B. David, A. Martin, H. P. Douglas and P. O'Brien, *Chem. Commun.*, 2006, 709.
42 J. Yang, H. I. Elim, Q. B. Zhang, J. Y. Lee and W. Ji, *J. Am. Chem. Soc.*, 2006, **128**, 11921.
43 J. H. Xiang, H. Q. Cao, Q. Z. Wu, S. C. Zhang and X. R. Zhang, *Cryst. Growth Des.*, 2008, **8**, 3935.
44 B. Ding, M. M. Shi, F. Chen, R. J. Zhou, M. Deng, M. Wang and H. Z. Chen, *J. Cryst. Growth*, 2009, **311**, 1533.
45 H. Sean, M. Stefan, L. Larissa, K. Ghada, Y. Jun, O. K. Shana and E. H. Sargent, *J. Am. Chem. Soc.*, 2007, **129**, 7218.
46 J. Aldana, Y. A. Wang and X. G. Peng, *J. Am. Chem. Soc.*, 2001, **123**, 8844.
47 A. L. P. Cornacchio and N. D. Jones, *J. Mater. Chem.*, 2006, **16**, 1171.
48 A. M. Derfus, W. C. W. Chan and S. N. Bhatia, *Nano Lett.*, 2004, **4**, 11.
49 R. Hardman, *Environ. Health Perspect.*, 2006, **114**, 165.
50 A. Hoshino, K. Fujioka, T. Oku, M. Suga, Y. F. Sasaki, T. Ohta, M. Yasuhara, K. Suzuki and K. Yamamoto, *Nano Lett.*, 2004, **4**, 2163.
51 A. M. Smith, H. Duan, A. M. Mohs and S. Nie, *Adv. Drug Delivery Rev.*, 2008, **60**, 1226.
52 A. Anas, H. Akita, H. Harashima, T. Itoh, M. Ishikawa and V. Biju, *J. Phys. Chem. B*, 2008, **112**, 10005.
53 Y. Jiang and Y. J. Zhu, *Chem. Lett.*, 2004, 1390.
54 K. S. Kim, S. Choi, J. H. Cha, S. H. Yeon and H. Lee, *J. Mater. Chem.*, 2006, **16**, 1315.

This journal is © The Royal Society of Chemistry 2010

J. Mater. Chem., 2010, **20**, 2336–2344 | 2343

55 N. O. Nunez and M. Ocana, *Nanotechnology*, 2007, **18**, 45.
56 E. K. Goharshadi, Y. Ding and P. Nancarrow, *J. Phys. Chem. Solids*, 2008, **69**, 2057.
57 J. Garcia-Serrano, U. Pal, A. M. Herrera, P. Salas and C. Angeles-Chavez, *Chem. Mater.*, 2008, **20**, 5146.
58 M. Behboudnia, A. Habibi-Yangjeh, Y. Jafari-Tarzanag and A. Khodayari, *Bull. Korean Chem. Soc.*, 2009, **30**, 53.
59 A. Yosra, J. Antonio, J. G. José, U. Marino and B. Gabriel, *J. Agric. Food Chem.*, 2007, **55**, 9646.
60 A. Bianco, A. Ramunno and Ed. Atta-ur-Rahman, *Stud. Nat. Prod. Chem.*, 2006, **33**, 859.
61 B. Armandodoriano, M. S. Anna and M. Cristiana, *ARKIVOC*, 2007, 146.
62 M. J. Amiot, A. Fleuriet and J. J. Macheix, *Photochemistry*, 1989, **28**, 67.
63 Y. Asaka, T. Kamikawa, T. Kubota and T. Sakamoto, *Chem. Lett.*, 1972, 141–144.
64 P. Gariboldi, G. Jommi and L. Verotta, *Phytochemistry*, 1986, **25**, 865.
65 H. Kuwajima, T. Uemura, K. Takaishi, K. Inoue and H. Inouye, *Phytochemistry*, 1988, **27**, 1757.
66 A. Bianco, S. R. Lo and M. L. Scarpati, *Phytochemistry*, 1993, **32**, 455.
67 A. Bianco, R. A. Mazzei, C. Melchioni, G. Romeo and M. L. Scarpati, *Food Chem.*, 1998, **63**, 461.
68 A. Bianco, R. A. Mazzei, C. Melchioni, M. L. Scarpati, G. Romeo and N. Uccella, *Food Chem.*, 1998, **62**, 343.
69 A. Bianco, C. R. Melchioni, G. Romeo and N. Uccella, *Nat. Prod. Res.*, 2004, **18**, 29.
70 A. Bianco, M. A. Chiacchio, G. Grassi, D. Iannazzo and R. Romeo, *Food Chem.*, 2006, **95**, 562.
71 A. Bianco, I. Muzzalupo, A. Piperno, G. Romeo and N. Uccella, *J. Agric. Food Chem.*, 1999, **4**, 3531.
72 A. Bianco, A. Piperno, G. Romeo and N. Uccella, *J. Agric. Food Chem.*, 1999, **47**, 3665.
73 K. G. U. Wijayantha, L. M. Peter and L. C. Otley, *Sol. Energy Mater. Sol. Cells*, 2004, **83**, 363.
74 L. Cademartiri, E. Montanari, G. Calestani, A. Migliori, A. Guagliardi and G. O. Ozin, *J. Am. Chem. Soc.*, 2006, **128**, 10337.
75 L. Turyanska, *Appl. Phys. Lett.*, 2007, **90**, 101913.
76 A. M. Lobo, T. Nagel, M. Borchert, H. Hickey and H. Weller, *J. Phys. Chem. B*, 2005, **109**, 17422.
77 J. J. Yeh and I. Lindau, *At. Data Nucl. Data Tables*, 1985, **32**(1), 1.
78 B. L. Wehrenberg, C. Wang and P. Guyot-Sionnest, *J. Phys. Chem. B*, 2002, **106**, 10634.
79 D. J. Bergman and M. Stockman, *Phys. Rev. Lett.*, 2003, **90**, 027402.
80 M. G. Bawendi, M. L. Steigerwald and L. E. Brus, *Annu. Rev. Phys. Chem.*, 1991, **41**, 477.
81 Y. Wang and N. Herron, *J. Phys. Chem.*, 1991, **95**, 525.
82 P. Weon, *Mater. Lett.*, 2003, **57**, 1508.
83 K. Tennakone, G. K. R. Senadeera, V. P. S. Perera, I. R. M. Kottegoda and L. A. A. Desilva, *Chem. Mater.*, 1999, **11**, 2474.
84 P. Hoyer and R. Konenkamp, *Appl. Phys. Lett.*, 1985, **3**, 66.
85 E. Cetinorgu, S. Goldsmith and R. L. Boxman, *Semicond. Sci. Technol.*, 1996, **21**, 364.
86 H. J. Yu and G. M. Choi, *Sens. Actuators, B*, 1999, **61**, 59.